3.3 THE FAA AWRP TURBULENCE PDT

R. Sharman*, L. Cornman, J. Williams
National Center for Atmospheric Research, Boulder, CO, 80307

S. Koch, W. Moninger
NOAA/ Earth System Research Laboratory/Global Systems Division, Boulder, CO, 80305

ABSTRACT

Commercial and general aviation aircraft continue to encounter unexpected turbulence that requires immediate changes to flight paths or is hazardous to the aircraft and passengers. This is due in part to the fact that current aviation-scale turbulence observations are inadequate and forecasts are not accurate enough to predict the location, time and intensity of turbulence. The FAA AWRP Turbulence Product Development Team (TPDT) addresses the turbulence under-measurement problem by researching, developing, and implementing new technologies for routine observations of turbulence (*in situ* and remote). It also researches and develops turbulence forecasting techniques that are aimed at providing operational forecasts of turbulence for the aviation community. This paper describes these three major work areas (*in situ* measurements, remote detection, and turbulence forecasting) for the Turbulence PDT.

1. Introduction

Encounters with turbulence for commercial (Part 121/129), air taxi (Part 135) and general aviation (GA, Part 91) aircraft pose significant safety, efficiency and workload issues. According to a recent MCR Federal survey of NTSB accident data for the years 1983-1997 (Eichenbaum, 1999), turbulence contributed to 664 accidents leading to 609 fatalities (mostly GA), 239 serious and 584 minor injuries, for an estimated average annual societal cost of $134 M. Although fatalities related to commercial airline turbulence encounters are almost nil (only one in this time period), turbulence encounters do account for a significant fraction (about 70%) of all weather related Part 121 incidents. The average number of air carrier turbulence-related injuries according to the NTSB records is about 45 per year, but these are of course only those that are reported to the NTSB. The actual numbers are probably higher: one major carrier reported almost 400 injury-causing turbulence encounters over a 3 year period; another estimated about 200 turbulence related customer injury claims per year.

A side effect to turbulence encounters is the perception by the public that air transportation is unsafe. Indeed, the number of pilot-reported/recorded encounters with turbulence is substantial: moderate-or-greater pilot reports (PIREPs) averaging about 65,000/year, and severe-or-greater PIREPs averaging about 5,500/year. For these reasons, more often than not, pilots will try to avoid or exit turbulent air, so turbulence also significantly impacts NAS (National Airspace) efficiency and controller workload.

In order to help reduce the number of turbulence encounters and their impact on the NAS, the FAA Aviation Weather Research Program (AWRP) sponsored Turbulence Product Development Team (TPDT) is working towards improving the detection and forecasting of turbulence, and providing operationally useful products directly to the users. The majority of the work has been done by the National Center for Atmospheric Research/Research Applications Laboratory (NCAR/RAL) and the NOAA/ Earth System Research Laboratory/Global Systems Division (ESRL/GSD, formally Forecast Systems Laboratory or FSL). Specifically, the TPDT has been focusing on three work areas: (1) providing *in situ* measurement and reporting of turbulence from commercial aircraft, and (2) the detection of in-cloud turbulence from the WSR-88D radar network, and (3) developing an automated turbulence forecasting system, (Graphical Turbulence Guidance or GTG). The research and development activities associated with each of these tasks will be addressed in separate sections below.

2. *In situ* detection of turbulence

Under the sponsorship of the FAA AWRP, work was begun in the early 1990's at the NCAR/RAL to develop and deploy an *in situ*

* Corresponding author address: Dr. Robert Sharman, National Center for Atmospheric Research, Research Applications Laboratory, Boulder,CO 80307; email: sharman@ucar.edu

turbulence measurement and reporting system for commercial aircraft. The concept was to use existing sensors, avionics and communication networks to produce and disseminate a state-of-the-atmosphere turbulence metric – the eddy dissipation rate (viz., $\varepsilon^{1/3}$, hereafter EDR). These data would then be used by a variety of users for operational and scientific purposes. Operational users include pilots, airline dispatch and meteorology personnel, aviation forecasters, and air-traffic personnel. Furthermore, these data would also be used by the turbulence research and development community for building and improving turbulence detection, nowcast and forecast products.

The EDR reports are intended to augment the existing turbulence pilot reporting data. As is well-known, these pilot reports are subjective measures of the aircraft's response to the turbulence, as opposed to quantitative, state-of-the-atmosphere measurements. Furthermore, pilot reports are sporadic in space and time, and very few null reports are made. The EDR reporting system was designed to address many of the deficiencies with pilot reports. That is, to provide routine and quantitative measurements of atmospheric turbulence intensity levels – including null reports. It should be noted that to save communications costs, some aircraft may be configured to generate EDR reports on an "event-driven," as opposed to routine basis.

Two principal algorithms have been developed to measure the eddy dissipation rate (EDR) from on-board data. The first method uses vertical accelerations and a mathematical model of the aircraft response to turbulence in order to estimate EDR values, whereas the second method uses a calculation of the vertical wind component. Starting in 1997, the implementation of the first-generation accelerometer-based EDR algorithm was begun on United Airlines aircraft. A total of 199 aircraft, B737s and 757s, currently have the algorithm installed; however, due to transmission cost concerns, only the 757s are currently providing routine EDR reports. Starting in 2006, the wind-based algorithm will be installed on 160 aircraft from Delta airlines and 400 aircraft from Southwest Airlines. In the following sections, a sampling of the current activities associated with the United Airlines deployment is discussed, including verification efforts and the use of the EDR reports in the development and verification of radar- and model-based turbulence products.

2.1 *Verification Activities*

The algorithm that has been implemented on the United Airlines aircraft is based on accelerometer data. Improvements to this first-generation accelerometer-based version exist, (including better aircraft response data, band-pass filtering and quality control processing), but have not been deployed. In fact, it is assumed that all future implementations will be based on the vertical wind, maximum-likelihood algorithm. Nevertheless, these accelerometer-based EDR data give a good idea as to the benefits of the turbulence reporting concept.

The EDR reports from the United Airlines deployment are undergoing verification by a comparison to pilot reports of turbulence as well as occasional passenger reports. Figure 2, Figure 1, and Figure 4 show a spatial series of EDR reports for portions of three different flights. These cases were chosen because there was a pilot report of turbulence from the specific flight. There are two locations indicated for the pilot reports: the red circle shows the location along the flight track at the time given in the pilot report; whereas, the black dot indicates the aircraft location given in the pilot report. Note that these two locations do not always match. The actual flight track is indicated by the color-coded (by altitude) diamonds and the two parallel tracks are the median and 95% $\varepsilon^{1/3}$ values, (color code in the upper right). The arrow gives the direction of the flight track.

In Figure 2, a reasonably good match is seen between the pilot report ("light-to-moderate") and the $\varepsilon^{1/3}$ report (0.25). There is a discrepancy between the locations of the encounter as given by the time in the pilot report versus the location given in the pilot report. In analyzing these data, it has been seen that this type of divergence occurs relatively often. Figure 1 illustrates a case where there is a difference between the pilot report ("light') and the $\varepsilon^{1/3}$ report (0.05). Without further information, this discrepancy cannot be resolved. However, it should be noted that since the $\varepsilon^{1/3}$ values are binned in increments of 0.1, an $\varepsilon^{1/3}$ value that lies between zero and 0.1 would be

reported as 0.05, and this could be a source of the difference. In future implementations, it is envisioned that a finer resolution, at least at the lower EDR values, might be employed. Finally, Figure 4 illustrates a more extreme example of the problem mentioned above regarding the positional inaccuracies in the pilot reports. The pilot report shown in this figure is from the same flight as the EDR reports. Nevertheless, the location of the aircraft given in the pilot report is over 100 km from the actual flight path. Besides all of the subjectivity inherent in the turbulence pilot reports, this type of inaccuracy is yet another motivation behind the deployment of the EDR reporting system.

Figure 3 and Figure present a comparison between EDR reports and turbulence "passenger reports" for two different flights. The passenger recorded a running evaluation of the turbulence intensity for the flights. The turbulence levels used by the passenger were: "null" (0), "null-to-light" (1), "light" (2), "light-to-moderate" (3), and "moderate" (4). Dashed lines between values indicate a constant intensity level between samples. In both examples, there is a reasonable, though not one-to-one correspondence between the passenger and EDR reports. As mentioned above, the coarse resolution between the EDR levels may contribute to some of this discrepancy. It has been noted that with this first version of the accelerometer-based EDR algorithm, it is not uncommon to find relatively large EDR values during the climb-out and approach phases of flight. This problem can clearly be seen in Figure 3. Furthermore, the on-board quality control algorithm often flags the EDR reports at these low altitudes (see the line just above the time field in the figures).

2.2 *Other Activities*

In 2006, a large number of Southwest Airlines B737 aircraft will have the wind-based i*n situ* algorithm deployed. The reports from these aircraft will complement those from the United Airlines aircraft, in terms of route structure. An uplink program with a select number of United Airlines aircraft will also occur during 2006. A character-based graphic product using the EDR data will be generated, uplinked and displayed on the ACARS printer.

An automated quality control algorithm for the *in situ* reports has been developed and implemented. These reports are now on an Experimental ADDS website, and are used by meteorologists and dispatchers at United Airlines. (see Figure 6).

3. Remote sensing of turbulence.

While the clear-air turbulence forecasts provided by GTG are now routinely generated, an automated system for identifying and disseminating information about hazardous convectively-induced turbulence remains lacking. This omission is particularly significant because historical data suggest that over 60% of turbulence-related aircraft accidents are due to convectively-induced turbulence (Cornman and Carmichael 1993). To address this issue, the NCAR Turbulence Detection Algorithm (NTDA) is being developed to provide a real-time capability for detecting potentially hazardous in-cloud turbulence using operational weather radars. The NTDA is a fuzzy-logic algorithm that uses radar reflectivity, radial velocity, and spectrum width to perform data quality control and compute atmospheric turbulence intensity estimates (eddy dissipation rate, EDR) and associated quality values, or confidences. A real-time demonstration of the NTDA using Level II data from sixteen NEXRADs in the upper Midwest was performed in the summer of 2005, producing a 3-D mosaic of in-cloud turbulence intensity at five-minute intervals. In addition, text-based maps of turbulence ahead were generated for all United Airlines aircraft in the demonstration domain, and were uplinked to the cockpit ACARS printers for select flights. This operational demonstration was the first step of a planned implementation that would offer turbulence detection over the conterminous United States, providing airline meteorologists, dispatchers, air traffic controllers, and pilots a new tool for identifying areas hazardous to aviation safety and helping to reduce delays and loss of capacity due to convective activity.

3.1 *NCAR Turbulence Detection Algorithm (NTDA)*

The NTDA is a fuzzy-logic algorithm that utilizes the radar reflectivity, radial velocity, and

spectrum width to perform data quality control and produce EDR estimates on the same polar grid as the raw radar data. A diagram of the algorithm is shown in Fig. 7. A data preprocessing step combines reflectivity and Doppler moment data from split cut tilts (e.g., lower elevation angles where the long-PRT reflectivity and short-PRT Doppler sweeps are commonly separate). Data quality control is performed in two steps: data censoring and data confidence computations. Data censoring removes measurements that are so contaminated by solar radiation and other sources as to be unusable. The confidence computations make use of an estimated signal-to-noise ratio (SNR), overlaid power ratio, Radar Echo Classifier clutter interest (Kessinger et al. 2003), spectrum width field "texture," radar reflectivity, measurement range from the radar and height above ground, and local averaging volume "coverage" by usable spectrum width data. An EDR estimate for each measurement point is computed by scaling the spectrum width by a theoretical quantity dependent on range (Cornman and Goodrich 1996), and local confidence-weighted averages are computed to produce the final EDR and confidence.

3.2 *Mosaicking technique*

The mosaicking algorithm works by collecting the latest data for each radar tilt in the domain of coverage. It computes the latitude, longitude and mean seal level (MSL) altitude of each relevant polar-coordinate radar data point, adjusting for beam bending using a standard model (Doviak and Zrnić 1993). It then loops through all the points on the desired 3-D Cartesian grid, computing a distance- and confidence-weighted average of the radar measurements near each location. The distance weighting function used in the operational demonstration is a 3-D Gaussian with a vertical standard deviation σ_v = 1,500 ft. and a horizontal standard deviation σ_h = 2 km. The averaging volume is truncated at 3 σ_v in the vertical and 4 σ_h in the horizontal to speed the computation. An associated distance-weighted average confidence is computed for each grid point using a similar formula. In creating reflectivity mosaics, the confidence of every radar reflectivity measurement is taken as 1.

3.3 *NTDA Operational Demonstration*

On 4 June 2005, a demonstration of an NTDA-based 3-D turbulence mosaic product that makes use of real-time Level II data from sixteen NEXRADs in the upper Midwest began. The demonstration domain covered a region from eastern Iowa and Missouri to western Pennsylvania and West Virginia and from southern Wisconsin and Michigan to northern Tennessee. Every 5 minutes, the most recent NTDA output from all the NEXRADs were combined into a 3-D mosaic having a horizontal resolution of 0.02° in latitude and longitude (approximately 2 km) and vertical levels at multiples of 3,000 ft. up to 45,000 ft. Radar reflectivity and NTDA confidence values were also mosaicked. A web-based Java display similar to the visualization tool in Experimental ADDS (http://www.weather.aero) allowed users to view the NTDA EDR, confidence, and reflectivity mosaics. Real-time *in situ* turbulence data obtained from United Airlines B-757 aircraft via the FAA's automated turbulence reporting system (Cornman et al., 1995 and 2004) could optionally be overlaid, as depicted in Fig. 8. For purposes of display, the EDR was scaled into a turbulence severity category of Smooth, Light, Moderate, Severe or Extreme based on its approximate hazard to a medium-sized aircraft flying at cruise speeds.

Another aspect of the real-time demonstration was the generation every five minutes of custom text-based maps of turbulence ahead for all United Airlines aircraft penetrating the demonstration domain (see Figure 9). Aircraft Situation Display to Industry (ASDI) data were used to determine the position and route of each aircraft and to predict its future path. NTDA mosaic data were then resampled onto a grid covering 114 nm ahead and 40 nm to either side of the predicted flight path, and turbulence hazard categories were represented by characters to produce the 2-D, text-based maps. The filed flight plan and relevant waypoints are also displayed. Messages containing significant turbulence are uplinked to the cockpit Aircraft Communications Addressing and Reporting System (ACARS) printers on select flights. A website allowed pilots to review all

generated messages and provide feedback for those that were uplinked.

3.4 *NTDA Verification Results*

In the early stages of development, the NTDA was verified and tuned using comparisons to EDR estimates calculated from research aircraft measurements obtained from various field programs. The recent availability of *in situ* EDRs from the FAA's automated turbulence reporting system (Cornman et al. 1995 and 2004) make a more comprehensive statistical evaluation possible. The *in situ* system downlinks one-minute average and peak EDR values. The 100 United Airlines B-757s equipped with this system supply several hundred flight hours per day of objective turbulence measurements in locations and conditions where commercial aircraft commonly fly. For the analysis presented here, comparisons were performed between the NTDA EDR and reflectivity mosaics generated between 5 June 2005 and 5 October 2005 and all valid *in situ* data reported in the demonstration domain at altitudes above 1,500 ft. The comparison was performed by computing the median of all mosaic values within 3,000 ft. vertically and 10 km horizontally of the aircraft path segment traversed during collection of an *in situ* EDR measurement.

Figure 10 shows box plots representing the distribution of NTDA EDR values corresponding to each of the one-minute average *in situ* EDR levels, which are quantized at 0.05 $m^{2/3}$ s^{-1} intervals and are listed across the *x*-axis. These comparisons show good correlation but substantial spread in the NTDA EDR estimates and a positive bias of about 0.15 $m^{2/3}$ s^{-1}. The spread may be due to time lags between the radar and aircraft measurements, the inherent difference between the two measurement systems, inhomogeneity over the mosaic comparison volumes, or inaccuracy in the *in situ* EDR reports. The bias may be due to inaccuracy in the *in situ* EDR reports, an incorrect choice of turbulence length scale, or the fact that the NTDA does not yet account for spectrum width estimator bias or spectral broadening mechanisms other than turbulence.

The Receiver Operating Characteristic (ROC) curves shown in Figure 11 illustrate the tradeoff between the probability of detecting *in situ* turbulence of various magnitudes vs. the probability of detecting the absence of turbulence (which is one minus the nuisance alarm rate). The fact that the curves approach the upper right corner of the plot indicates that the NTDA has skill in predicting aircraft turbulence encounters. In addition, the fact that the NTDA performs better for higher levels of turbulence is encouraging. For example, an 80% PoD of moderate turbulence would incur a 34% nuisance alert rate. (Note, however, that the red line representing the ROC curve for severe or greater turbulence is not meaningful, since only two severe turbulence measurements were available for comparison.) These results are very promising, especially considering the difficulties in comparing the NTDA and aircraft measurements, which are measured over different volumes and often at times differing by several minutes.

In contrast, an identical comparison of median radar reflectivity mosaic values with *in situ* average EDR measurements showed that radar reflectivity exhibited no skill in predicting turbulence intensity. This is a noteworthy result, since reflectivity magnitude is often used by pilots, dispatchers and others to assess the likelihood of convectively-induced turbulence hazardous to aircraft. Of course, these data were collected from actual commercial flights, which tend to avoid penetrating thunderstorms and other areas of enhanced reflectivity. Nevertheless, this analysis suggests that the NTDA EDR is potentially a more useful metric of turbulence hazard than reflectivity magnitude is.

3.5 *Future Work*

Efforts are currently underway to refine the NTDA, with the goal of further improving its performance. Case studies are being performed of events in which a significant mismatch between the NTDA and *in situ* EDR values are observed, and the many parameters in the algorithm are being empirically tuned. The use of radial velocity measurements via a structure-function approach is also being investigated. It is anticipated that these algorithm improvements will be highlighted in a second real-time demonstration to be performed in the summer of 2006.

In collaboration with the Advanced Weather Radar Techniques PDT, the NTDA is being

implemented in the NEXRAD Open Radar Products Generator (ORPG) Common Operations and Development Environment. If approved for implementation on all NEXRADs, EDR data will become part of the NEXRAD Level III data stream, available to all interested users for operational or scientific purposes. In particular, these data could be used to generate a nationwide real-time turbulence detection product similar to the 3-D mosaic produced during the summer 2005 demonstration. Such a product could provide both strategic and tactical turbulence hazard information to aviation meteorologists, airline dispatchers, pilots, general aviation users, and air traffic controllers. The in-cloud turbulence product would supplement radar reflectivity and GTG in assessing the likelihood of hazardous in-cloud turbulence. Eventually, it is anticipated that the NTDA output will be combined with satellite, *in situ*, and NWP model data to identify and forecast regions of hazardous convectively-induced turbulence. The resulting turbulence "nowcast" capability could significantly improve aviation safety and air traffic flow during convective events.

4. Turbulence forecasting

The MCR Federal report mentioned in the introduction (Eichenbaum, 1999) estimated that *only about 30% of upper level injury-causing turbulence incidents were forecast based on previous turbulence PIREPs or valid AIRMETs.* A large percentage of these turbulence encounters might be avoided if better turbulence forecast products were available for use by air traffic controllers, airline flight dispatchers, and flight crews. Strategic planning for turbulence avoidance can be accomplished if sufficiently accurate forecasts of turbulence are available. Previous studies (e.g., Fahey 1993) have shown that at least for commercial air carriers, strategic planning can reduce cabin injuries and reduce carrier costs. However, current forecasting methods have not generally provided acceptably high detection rates and at the same time acceptably low false alarm rates. The term "acceptable" does not have a universal quantitative definition, but the Turbulence Joint Safety Implementation Team (JSIT) report to improve the quality of turbulence information recommended probabilities of MOG detection should be > 0.8 and probabilities of null detection should be > 0.85 for turbulence forecasts to be most useful.

The lack of progress in the turbulence forecasting area is due in large part to the fact that, from the meteorological perspective, turbulence is a "microscale" phenomenon. In the atmosphere, turbulent "eddies" are contained in a spectrum of sizes, from 100s of kilometers down to centimeters. But aircraft bumpiness is most pronounced when the size of the turbulent eddies encountered are about the size of the aircraft; for commercial aircraft this would be eddy dimensions of about 100m or so. It is impossible to directly forecast atmospheric motion at this scale (it would take about 10m resolution with a grid-based forecast model), now or even in the foreseeable future. Fortunately, it appears that most of the energy associated with eddies of this scale cascades down from the larger scales of atmospheric motion (e.g. Dutton and Panofsky, 1970), which may in fact be resolved by current weather observations and numerical forecast models. Assuming the large-scale forecasts are sufficiently accurate, the turbulence forecasting problem is then one of identifying large-scale features that are conducive to the formation of aircraft scale eddies. So one major area of research over the last 50 years or so has involved efforts to establish a linkage between large-scale atmospheric features (i.e., observable by routine meteorological observations and resolvable by numerical weather prediction models) and aircraft-scale turbulence. Some of these linkages have been inferred through the efforts of National Weather Service and airline meteorological forecasters as turbulence forecasting rules-of-thumb, but the skill depends on the forecaster, and that skill diminishes rapidly with forecast lead time.

The TPDT recognizes the need for automated reliable turbulence forecasts, and that need is being addressed in two ways. First, applying the results of turbulence-related research to the development of an automated turbulence diagnosis and forecasting system, termed the GTG (Graphical Turbulence Guidance). The GTG has been implemented on the NCEP operational ADDS (Aviation Digital Data Service) website (http://adds.aviationweather.gov/turbulence) and produces 4-D grids of turbulence potential using RUC model forecast grids. Second, given that

turbulence forecasting progress is hampered by our incomplete understanding of the causes and life cycles of atmospheric turbulence, the TPDT devotes some of its resources towards research that leads to better understanding of the generation and evolution processes of turbulence.

4.1 *GTG status*

The automated turbulence forecasting system developed by the TPDT was originally named the Integrated Turbulence Forecasting Algorithm, ITFA, and concentrated only on upper level (>FL200) clear-air turbulence (see Sharman et al., 1999, Sharman et al., 2000, Sharman et al., 2002, Tebaldi et al., 2002). In brief, the essence of the technique is to combine many different turbulence diagnostics in an optimal way to account for current observations (PIREPs). The diagnostics are aimed mainly at identifying clear-air turbulence (CAT) potential related to upper-level fronts and jet streams. Mountain wave turbulence and convective sources of turbulence are not explicitly accounted for, but may be captured by some of the more "generic" turbulence diagnostics. This approach of dynamically assigning weights has been shown by Tebaldi et al. (2002) to give better performance than using a single diagnostic.

The ITFA system became "operational" for qualified meteorologists and dispatchers in March 2003 and at that time was renamed the Graphical Turbulence Guidance (GTG) product. The first generation GTG, or GTG1, provides gridded CAT forecasts stratified by flight levels and graphical displays of turbulence potential are provided on those flight levels to interested users at the ADDS website. An example of GTG1 output as provided on the ADDS website is shown in Fig. 12.

The next generation of GTG, GTG2, is currently under final testing and is expected to be deployed on the operational ADDS website in late 2006. GTG2 expands the capabilities of GTG1 by extending turbulence analyses and forecasts down to FL100 from the GTG1 value of FL200. The FL100-FL200 altitude band is especially significant for air taxi commercial carriers. Thus in the new system, there are turbulence predictions at both upper levels (≥FL200) and mid-levels (FL100-FL200). In addition, some new turbulence diagnostics were included as a result of continued turbulence diagnostic research by the TPDT and other researchers. A detailed description of the GTG2 product is provided in Sharman et al. (2004). Both subjective and objective evaluations of the ITFA/GTG based on comparisons to available turbulence reports (or pilot reports, PIREPs) have been an integral part of the algorithm's development since its inception. Independent *subjective* evaluations have been made by the Aviation Weather Center (AWC), the FAA's William J. Hughes Technical Center, and various airlines. *Objective* evaluations based on comparisons to PIREPs have been ongoing by both the developers and an independent verification team composed of scientists from NOAA-Research-ESRL/GSD and NCAR/RAL. Results of the evaluations from previous years can be found in Brown et al. (2000). Complete objective evaluations in the form of probability of detection (POD) statistics are also available on a daily basis on NOAA-Research-ESRL/GSD's Real-Time Verification System (RTVS) (see Mahoney et al. 2002 for a description) website (http://www-ad.fsl.noaa.gov/fvb/rtvs) since 1999.

Both subjective and objective evaluations are performed independently by the Quality Assessment (QA) PDT (see Mahoney and Brown 2006) and are input to the FAA/NCEP Aviation Weather Technical Transfer (AWTT) process. The AWTT board is set up to guide and accelerate transition of aviation weather R&D products into operations, while ensuring that GTG or any FAA AWRP product is accurate, useful, and operationally robust. Assisting the AWTT Board is the AWTT Steering Group (ASG), composed of FAA and NWS personnel in the Board members' organizations who are knowledgeable in the areas relevant to the particular product being evaluated. The ASG with inputs from the QAPDT evaluates the product on its scientific merits and accuracy and submits its recommendations for advancement of the product to the next decision point to the AWTT Board, who after consulting with relevant user groups approves or disapproves the decision point for the product. The Board applies a four-point set of decision criteria (D1, D2, D3, D4) successively at various stages of the technology transfer cycle. In particular, a QAPDT independent verification report accompanies the transition to D3 ("Experimental") or D4 ("Operational") of GTG or any FAA AWRP product. After a D3 approval the experimental

product is available to the public through the Experimental ADDS display for preliminary evaluations; and after a D4 approval the product is available on Operational ADDS to qualified meteorologists and dispatchers as an aid to making routing decisions.

One of the objective measures of diagnostic/GTG performance used by both the GTG development team and the QAPDT is the area under PODY-PODN ROC curves (AUC), as demonstrated for the NTDA performance. In this procedure a set of thresholds is assumed for each diagnostic and the GTG combination, and for each threshold the diagnostic performance based on comparisons to available turbulence PIREPs is evaluated by computing both a PODN and a PODY. Here PODN refers to the probability of detection of "null" or smooth turbulence events, and PODY refers to the probability of detection of moderate-or-greater (MOG) turbulence events. These curves essentially measure the ability of a forecast algorithm to discriminate between Yes (i.e. MOG) and No (i.e. smooth) turbulence events. For the range of thresholds selected, higher combinations of PODY and PODN, and therefore larger AUCs, imply greater skill in discriminating between null and MOG turbulence events. The AUC ranges from 0.5 for no skill to 1.0 for perfect skill. For a more complete discussion of the use of the AUC as a discrimination metric see e.g. Marzban (2004). ROC curves derived for the 6-hr forecast performance for GTG2 and its component algorithms based on one years' worth of PIREP data are shown in Fig. 13. As can be seen, by this measure, GTG2 outperforms its constituent diagnostics and AIRMETs for both mid- and upper-levels.

In addition, UAL *in situ* reports will be included in the GTG2 product. This provides considerably more null reports, and removes much of the uncertainty associated with using PIREPs for tuning and verification. The strategies for incorporating *in situ* data in GTG2 are discussed elsewhere in this volume (Abernethy and Sharman 2006), but a sample of the expected increase in ROC performance using a simple UAL bin-PIREP mapping is provided in Fig. 14.

Future versions of GTG will include other known sources of turbulence such as mountain-wave-induced turbulence (MWT) and convectively-induced turbulence (CIT), as well as new data sources of turbulence measurements as they become available. Table I lists the projected schedule of future GTG releases.

4.2 *Turbulence diagnostic research*

This is a continued research area for the TPDT as well as for other major laboratories and universities. But any diagnostic must be judged by its overall performance, not just on a few select cases. Diagnostic performance may be conditional, and information about when a particular diagnostic performs well and when it does not, could be used in dynamically assigning its weight within the GTG framework. Hopkins (1977) and Lester (1994) describe synoptic conditions which are known to be conducive to CAT, and these could be developed into automated algorithms.

Although some of the current diagnostics are independent of the source of turbulence, most are tuned for CAT associated with fronts and enhanced wind shears in the vicinity of jet streams. Exceptions include a) diagnostics developed by the Turbulence PDT members using second-order structure functions evaluated on RUC model velocity fields to infer turbulence (Frehlich and Sharman 2004a, 2004b), and b) gravity wave diagnostics related to "Unbalanced Flow" (as defined by the nonlinear balance equation) associated with the jet stream (Koch and Caracena 2002; Koch et al. 2005). Diagnostics specific to other sources of turbulence, e.g., those related to deep convection, must be also developed, tested and implemented into future versions of GTG. Turbulence related to convection has been shown by Kaplan et al. (2005) to be coincident with some particularly severe encounters.

From recent investigations by TPDT members it is now apparent that gravity waves and their breakdown play a crucial role in turbulence generation processes in both clear-air associated with jet streams (Lane et al. 2004, Lane et al. 2005, Koch et al. 2005) and near deep convection (Lane et al. 2003). Thus the relation of gravity waves (which are for the most part not resolved by current NWP models) to the large (resolved) scale atmospheric structure and the processes by which gravity waves, once generated, may break down

into turbulence are areas of concentration by the TPDT.

As an example, an extension of the Lane et al (2003) study has shown that the gravity waves and turbulence produced in the stratosphere above deep convection depend on the stability and wind shear near the cloud top, since these environmental parameters directly impact gravity wave propagation characteristics. Figure 15 demonstrates this effect.

Other sources for convectively-generated turbulence are also being investigated. For example, ongoing analysis of special dropsonde and P-3 airborne Doppler radar data analyses collected on multiple severe thunderstorm events during the Bow Echo and Mesoscale Convective Vortex Experiment (BAMEX) indicates that strong vertical wind shear associated with a descending rear inflow jet beneath the large convective "anvil cloud" is highly conducive to the generation of strong turbulence (Collander et al. 2006). Power spectral density analyses of the P-3 data show a slope typical of the turbulence subrange at wavelengths smaller than ~300 m, and second-order structure function analysis of this aircraft wind data indicates a sudden change in slope between the turbulence scales and the gravity waves (scales larger than 300 m), allowing for a clear separation of the two phenomena. Though these results are primarily observational and exploratory in nature, it is hoped that this work will lead to a quantitative assessment of the turbulence threat to general aviation and passenger airlines in the vicinity of anvil regions produced by mesoscale convective systems. However, this will not be a simple task; in particular, wind profiles from the RUC model made in the vicinity of the observed rear inflow jets in the BAMEX cases do not, in general, depict the presence of this jet and the associated small Richardson Number profile. The nature of this difference and that of other features in the remaining quadrants remains to be determined with refined composite and/or analysis procedures, but the most obvious problem appears to be RUC deficiencies in forecasting some important aspects of mesoscale convective systems, suggesting much work will be needed to improve the predictability of convectively-induced turbulence.

Spectral analysis of NOAA Gulfstream-IV in situ data shows that turbulence may occur in areas closely related to upper-level gravity-wave activity but apart from regions of large vertical wind shear (Koch et al. 2005). These findings are consistent with the underlying foundation for the Unbalanced Flow (UBF) diagnostic (Koch and Caracena 2002): a) dynamical imbalance associated with an upper-level jet results in the generation of a packet of gravity-inertia waves with horizontal wavelengths of 100–200 km, b) vertical wind shear is increased and static stability reduced as the waves become steeper and their horizontal wavelengths are shortened due to nonlinearity, and c) turbulence is generated as these waves break. Wavelet and third-order structure function analysis of the aircraft in-situ observations also indicates a close causality relationship between gravity waves and turbulence (Lu et al. 2005a, b), notably that turbulence is generated quite suddenly as the degree of coherence and polarity of the gravity waves exceeds a certain value. The ability to predict the forcing mechanisms for gravity waves associated with the upper-level jet and the wave characteristics (amplitude, wavelength, phase speed), plus improved understanding of how such relatively large-scale wave phenomena could produce conditions necessary for turbulence to be generated at scales < 1 km are all essential for making substantial progress on predicting clear-air turbulence with operational numerical weather prediction models.

Since the basic process by which gravity-inertia waves create conditions suitable for turbulence to occur, and the conditions under which such a process may or may not develop are not well understood, the Turbulence PDT is currently conducting more controlled, idealized studies of the process by which jet imbalance may spawn gravity waves, and how such waves may culminate in the generation of turbulent kinetic energy of sufficient intensity that it could be disruptive to commercial aircraft. We are using the WRF model initialized with an initially balanced three-dimensional baroclinic wave and multiple grid nests to simulate the upper-level jet, mesoscale gravity waves, and turbulence, beginning at a horizontal grid spacing of 100 km and nesting all the way down to 250 m. Our results show a cascade of gravity wave energy,

beginning with the ~100-200 km scale gravity-inertia waves produced by jet stream imbalances (Fig. 16), followed by breaking internal waves with wavelengths of 10-30 km, and finally, the generation of turbulence (Lu et al. 2006). The interaction between these various phenomena, having a wide range of wavelengths, amplitudes, and phase velocities is very complex and will require further investigation. However, the ultimate goal is to be able to map out the parameter space that determines these gravity wave characteristics in a highly predictable manner, so that the probability of turbulence generation may be determined and thereby predicted.

Recently, the TPDT has begun to evaluate the situation-dependent performance of GTG component algorithms for forecasts of upper- and mid-level turbulence, the objective being to try to improve the performance of GTG even further. This work involves performing in-depth analyses of the meteorological conditions under which selected indices and algorithms within GTG do and do not perform well, in order to be able to create a set of rules for codifying algorithm performance as a function of meteorological conditions and model performance for use in GTG.

5. Summary

Encounters with turbulence for commercial and GA aircraft pose significant safety, efficiency and workload issues. More often than not, pilots will try to avoid or exit turbulent air, so turbulence significantly impacts NAS efficiency and controller workload. Fortunately, not every significant encounter with turbulence results in an injury, nevertheless, according to NTSB numbers, each year, turbulence accounts for approximately 60-70% of all weather-related accidents and incidents. The cost to US airlines due to injuries (medical attention and liability suits), cabin and aircraft damage, flight delays, and time lost to inspection and maintenance is substantial, with estimates in the $150-$500 million/year range.

In order to help reduce the number of turbulence encounters and their impact on the NAS, the FAA AWRP Turbulence PDT is working on improving the detection and forecasting of turbulence, and providing operationally useful products directly to the users. To this end the Turbulence PDT has been focusing and will continue to focus on three major work areas:

- Automated *in situ* reporting. Providing automated, quantitative, and aircraft-independent *in situ* reports of turbulence from commercial aircraft. Currently 200 aircraft from United Airlines have the *in situ* turbulence software deployed, with approximately 1.3 million reports being generated every month - compared to approximately 55,000 PIREPs per month. Work has been ongoing with Southwest Airlines to equip their fleet of 737 aircraft.
- Automated turbulence forecasting. Over the last several years NCAR has developed a turbulence diagnosis and forecast system for the continental U.S. This system, GTG, which has been part of the NCEP ADDS operational suite since March 2003, produces a 4-D grid of turbulence potential for clear-air turbulence above 20,000 ft MSL using RUC model forecast grids. GTG2 will extend the diagnoses and forecasts down to 10,000 MSL and should become operational in late 2006. Research and development of new turbulence diagnostics is an ongoing effort.
- In-cloud turbulence detection. A new turbulence detection algorithm designed for use on the WSR-88D radars has been developed and is being tested (NTDA). Uplink to the cockpit of selected UAL aircraft during summer 2005 have demonstrated the utility of this product in increasing pilot situational awareness of turbulence within convection.

The outlets for these work areas are turbulence strategic and tactical decision avoidance aids to be used by the aviation community. Strategic avoidance is provided by the GTG forecasts, which incorporates *in situ* data and will also eventually incorporate NTDA output for nowcasts. Tactical avoidance of turbulence in cloud is provided by the NTDA. It is envisioned that soon NTDA, in situ and GTG output will be uplinked to the cockpit for better pilot situational awareness.

Acknowledgments. This research is in response to requirements and funding by the Federal

Aviation Administration (FAA). The views expressed are those of the authors and do not necessarily represent the official policy or position of the FAA.

REFERENCES

Abernethy, J. and R. Sharman, 2006: Clear-air turbulence nowcasting and forecasting using in situ turbulence data. Preprints, *Twelveth Conf. on Aviation, Range, and Aerospace Meteorology*, Atlanta, GA, Amer. Meteor. Soc., P1.5.

Brown, B. G., G. Thompson, R.T. Bruintjes, R. Bullock, and T. Kane, 1997: Intercomparison of in-flight icing algorithms. Part II: Statistical verification results. *Wea. Forecasting*, **12**, 890-914.

Brown, B. G., J. L. Mahoney, J. Henderson, T. L. Kane, R. Bullock, and J. E. Hart, 2000: The turbulence algorithm intercomparison exercise: Statistical verification results. Preprints, *Ninth Conf. on Aviation, Range, and Aerospace Meteorology*, Orlando, FL, Amer. Meteor. Soc., 466-471.

Collander, R. S., E. Tollerud, B. Jamison, F. Caracena, C. Lu, and S. E. Koch, 2006: Turbulence in MCS anvils: observations and analyses from BAMEX. Preprints, *12th Conf. on Aviation, Range, and Aerospace Meteorology*, Atlanta, GA, Amer. Meteor. Soc.

Cornman, L. B., C. S. Morse, and G. Cunning, 1995: Real-time estimation of atmospheric turbulence severity from in-situ aircraft measurements. *J. Aircraft*, **32,** 171-177.

Cornman, L. B. and B. Carmichael, 1993: Varied research efforts are under way to find means of avoiding air turbulence. *ICAO Journal*, 48, 10-15.

Cornman, L. B., and R. K. Goodrich, 1996: The detection of atmospheric turbulence using Doppler radars. Preprints, *Workshop on Wind Shear and Wind Shear Alert Systems*. Oklahoma City, 13-15 November. Amer. Meteor. Soc., Boston.

Cornman, L. B., G. Meymaris, and M. Limber, 2004: An update on the FAA Aviation Weather Research Program's *in situ* turbulence measurement and reporting system. Preprints, *Eleventh Conf. on Aviation, Range, and Aerospace Meteorology*, Hyannis, MA, Amer. Meteor. Soc., P4.3.

Doviak, R. J., and D. S. Zrnić, 1993: *Doppler Radar and Weather Observations*. Academic Press, 562 pp.

Dutton, J., and H. A. Panofsky, 1970: Clear Air Turbulence: A mystery may be unfolding. *Science*, **167**, 937-944.

Eichenbaum, H., 2000: Historical overview of turbulence accidents. MCR Federal, Inc. report TR-7100/023-1.

Fahey, T. H., 1993: Northwest Airlines atmospheric hazards advisory and avoidance system. Preprints, *Fifth Conf. on Aviation Weather Systems*, Vienna, VA, Amer. Meteor. Soc., 409-413.

Frehlich, R., and R. Sharman, 2004a: Estimates of turbulence from numerical weather prediction model output with applications to turbulence diagnosis and data assimilation. *Mon. Wea. Rev*., **132**, 2308-2324.

Frehlich, R., and R. Sharman, 2004b: Estimates of upper level turbulence based on second order structure functions derived from numerical weather prediction model output. Preprints, *Eleventh Conf. on Aviation, Range and Aerospace Meteorology,* Hyannis, MA, Amer. Meteor. Soc., P4.13.

Hopkins, R. H., 1977: Forecasting techniques of clear-air turbulence including that associated with mountain waves. WMO Technical Note No. 155, 31 pp.

Kaplan, M. L, A. W. Huffman, K. M. Lux, J. J. Charney, A. J. Riordan, and Y.-L. Lin, 2005: Characterizing the severe turbulence environments associated with commercial aviation accidents. Part 1: A 44-case study synoptic observational analyses. *Meteor. Atmos. Phys*.**,88**, 129-153.

Kessinger, C., S. Ellis and J. Van Andel, 2003: The radar echo classifier: a fuzzy logic algorithm for the WSR-88D. Preprints-CD, *3rd AMS Conference on Artificial Intelligence Applications to Environmental Science*, Long Beach, 9-13 Feb.

Koch, S. E., and F. Caracena, 2002: Predicting clear-air turbulence from diagnosis of unbalance

flow. Preprints, *Tenth Conf. on Aviation, Range, and Aerospace Meteorology*, Portland, OR, Amer. Meteor. Soc., 359-363.

Koch, S. E., B. D. Jamison, C. Lu, T. L. Smith, E. I. Tollerud, C. Girz, N. Wang, T. P. Lane, M. A. Shapiro, D. D. Parrish, and O. R. Cooper, 2005: Turbulence and gravity waves within an upper-level front. *J. Atmos. Sci.,* **62,** 3885-3908**.**

Lane, T.P., R.D. Sharman, T.L. Clark, and H.-M. Hsu, 2003: An investigation of turbulence generation mechanisms above deep convection. *J. Atmos. Sci.*, **60**, 1297-1321

Lane, T. P., J. D. Doyle, R. Plougonven, M. A. Shapiro, and R. D. Sharman, 2004: Observations and numerical simulations of inertia-gravity waves and shearing instabilities in the vicinity of a jet stream. *J. Atmos. Sci*., **61**, 2692-2706.

Lane, T.P., R. Sharman, H.-M. Hsu, W. D. Hall, M. A. Shapiro, R. Plougonven, and J. J. Murray, 2005: Numerical simulations of gravity waves and turbulence during the ATReC campaign. **AIAA-2005-262**. *43rd AIAA Aerospace Science and Exhibit*, Reno, NV.

Lester, P. F., 1994: *Turbulence: A new perspective for pilots*. Jeppesen Sanderson, Inc., 212 pp.

Lu, C., S. E. Koch, and N. Wang, 2005a: Determination of temporal and spatial characteristics of atmospheric gravity waves combining cross-spectral analysis and wavelet transformation. *J. Geophys. Res*. **110,** D01109, doi:10.1029/2004JD004906.

Lu, C., S. E. Koch, and N. Wang, 2005b: Stokes parameter analysis of turbulence-generating gravity waves combining cross-spectral analysis and wavelet transformation. *J. Geophys. Res*., **110,** doi:10.1029/2004JD005736.

Lu, C., W. D. Hall, and S. E. Koch, 2006: High-resolution numerical simulations of gravity wave-induced turbulence in association with an upper-level jet system. Preprints*, 12th Conf. on Aviation, Range, and Aerospace Meteorology*, Atlanta, GA, Amer. Meteor. Soc.

Mahoney, J. L and B. G. Brown, 2006: The FAA Aviation Weather Research Quality Assessment Product Development Team. Preprints, *Twelveth Conf. on Aviation, Range, and Aerospace Meteorology*, Atlanta, GA, Amer. Meteor. Soc., P1.24.

Mahoney, J. L, J. K. Henderson, B. G. Brown, J. E. Hart, A. Loughe, C. Fischer, and B. Sigren, 2002: The Real-Time Verification System (RTVS) and its application to aviation weather forecasts. Preprints*, Tenth Conf. on Aviation, Range, and Aerospace Meteorology*, Portland, OR, Amer. Meteor. Soc., 323-326.

Marzban, C., 2004: The ROC curve and the area under it as performance measures. *Wea. Forecasting*, **19**, 1106-1114.

Sharman, R., C. Tebaldi, and B. Brown, 1999: An integrated approach to clear-air turbulence forecasting. Preprints*, Eighth Conf. on Aviation, Range, and Aerospace Meteorology*, Dallas, TX, Amer. Meteor. Soc., 68-71.

Sharman, R., C. Tebaldi, J. Wolff, and G. Wiener, 2002: Results from the NCAR Integrated Turbulence Forecasting Algorithm (ITFA) for predicting upper-level clear-air turbulence. Preprints, *Tenth Conf. on Aviation, Range, and Aerospace Meteorology*, Portland, OR, Amer. Meteor. Soc., 351-354.

Sharman, R., J. Wolff, and G. Wiener, 2004: Description and evaluation of the second generation Graphical Turbulence Guidance forecasting system. Preprints, *Eleventh Conf. on Aviation, Range, and Aerospace Meteorology*, Hyannis, MA, Amer. Meteor. Soc., 4.14.

Tebaldi, C., D. Nychka, B. G. Brown, and R. Sharman, 2002: Flexible discriminant techniques for forecasting clear-air turbulence. *Environmetrics 2002*, **13**, 859-878.

Table 1. Scheduled GTG releases, corresponding capabilities, and AWTT D3, D4, and operational implementation timelines

Version	Capabilities	D3	D4	Operational
GTG1	Upper levels RUC20	---	3/03	3/03
GTG2	Improved GTG1 Mid levels RUC13 Text generation Uses in situ	11/04	05/06	8/06
GTG3	Improved GTG2 MWT 10 km RR WRF Probabilistic forecasts	11/07	11/08	2/09
GTG/TFO	Global - GFS	11/07	11/08	2/09
GTG4	Improved GTG3 out-of-cloud turb forecasts	11/08	11/09	2/10
GTGN	Rapid upates in-cloud turb nowcasts in situ GTG4 0-2 hr analyses	11/08	11/09	2/10
GTG5	Improved GTG4 Low levels	11/09	11/10	2/11

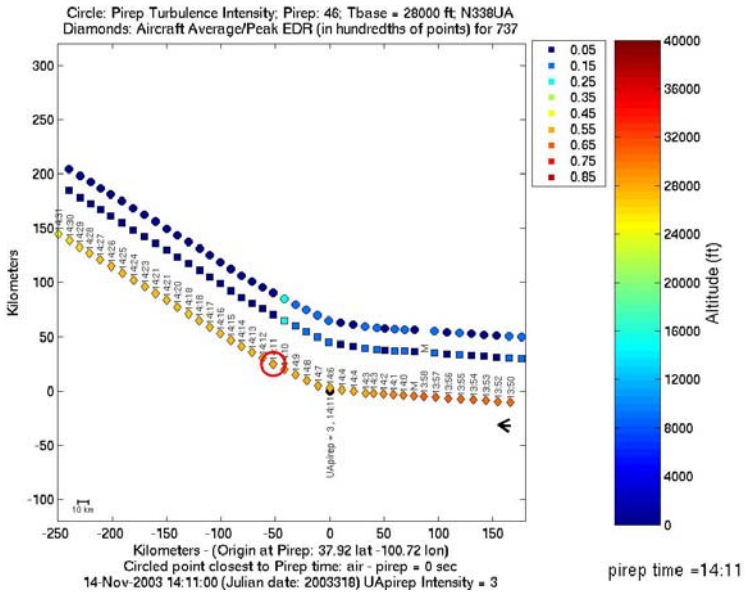

Figure 2. Spatial series of EDR reports illustrating a good match between the pilot report (“light-to-moderate”) and the EDR values.

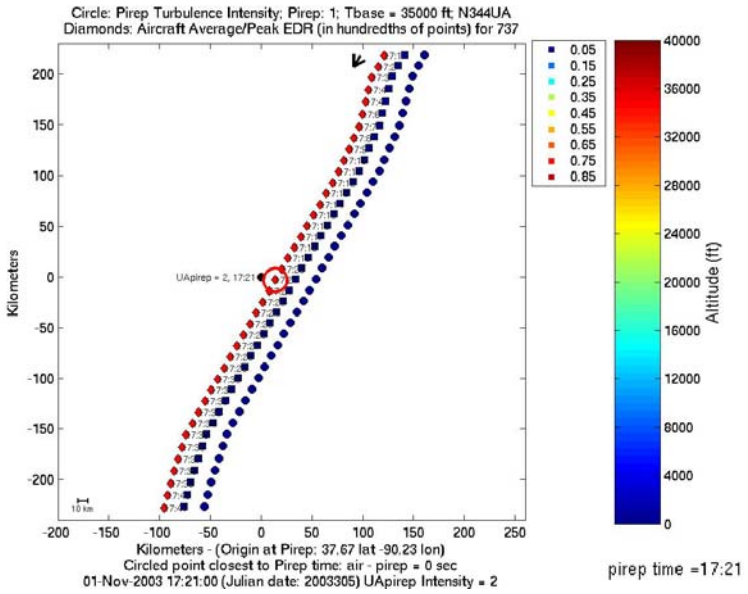

Figure 1. Spatial series of EDR reports illustrating a discrepancy between the pilot report (“light”) and the EDR values.

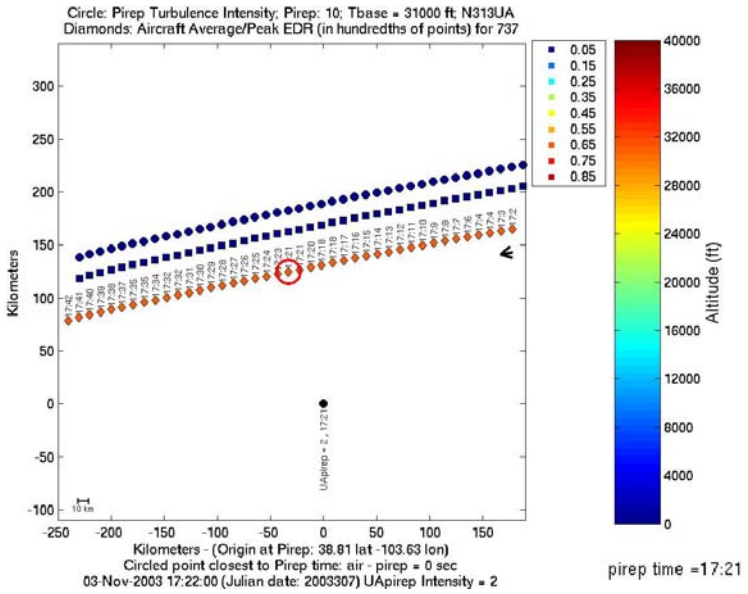

Figure 4. Spatial series of EDR reports illustrating one of the problems in using pilot reports for verification work. The location given in the pilot report is approximately 100 km from the actual flight track.

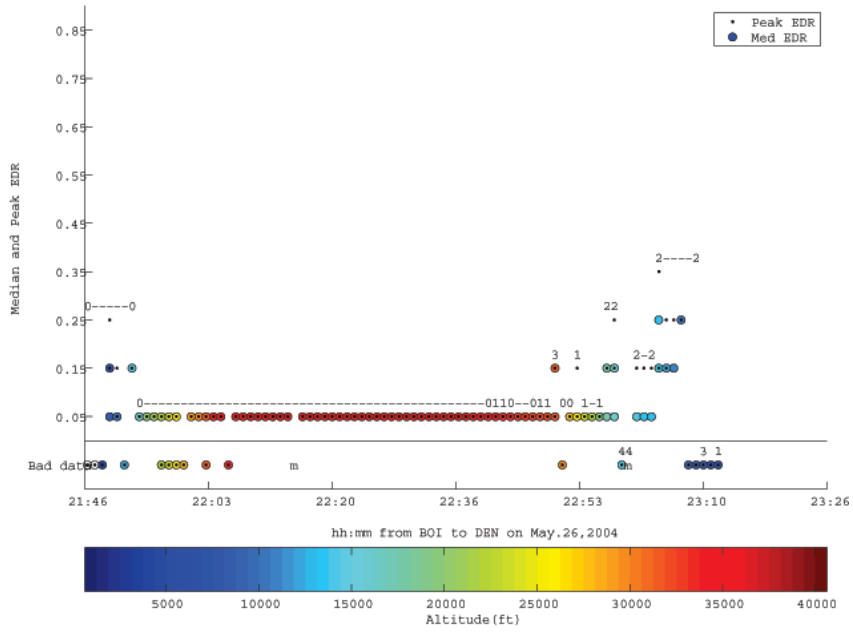

Figure 3. Comparison between EDR reports and “passenger reports.”

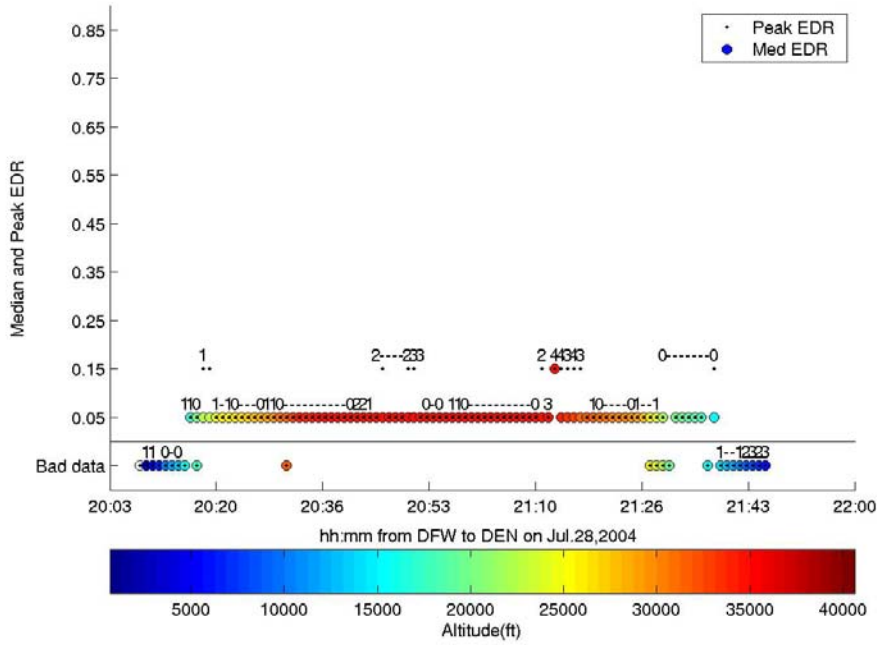

Figure 5. Comparison between EDR reports and "passenger reports."

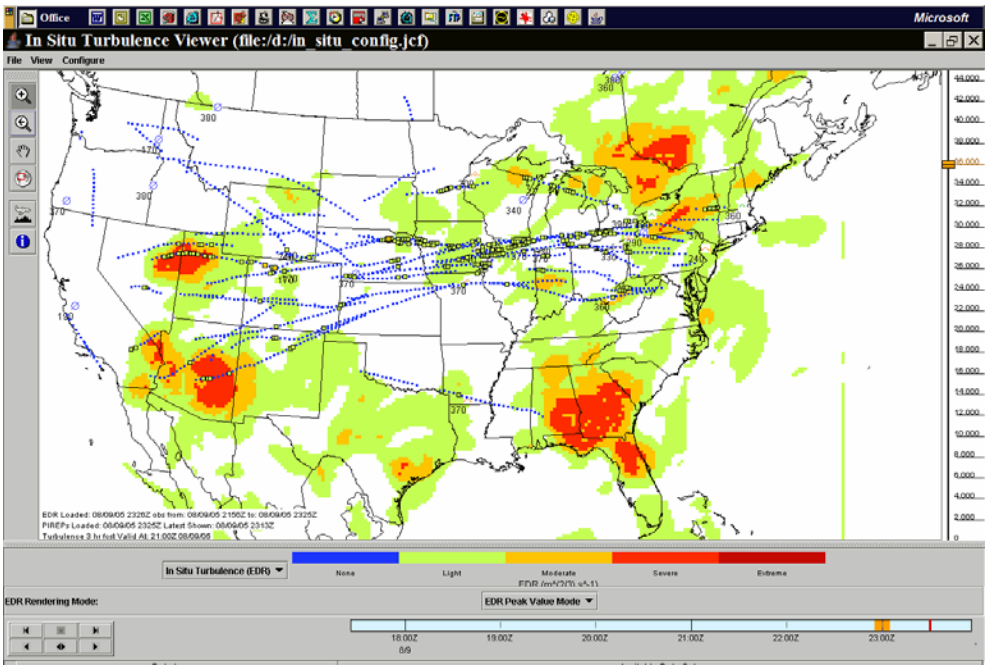

Figure 6. Experimental ADDS Web-based display showing *in situ* turbulence reports overlaid on contours of the Graphical Turbulence Guidance (GTG) turbulence forecast product.

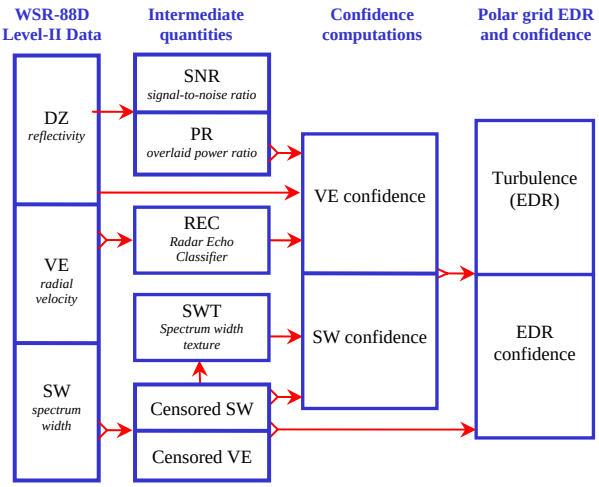

Figure 7: Diagram of the NTDA, as implemented for the WSR-88D (NEXRAD) radar. The Level II reflectivity, radial velocity and spectrum width data are used to censor bad data and compute EDR and an associated confidence for each radar measurement point via a fuzzy-logic framework. A pre-processing step that isn't shown merges split-cut tilts (e.g., surveillance and Doppler sweeps) so that the reflectivity, radial velocity, and spectrum width data are on a common grid.

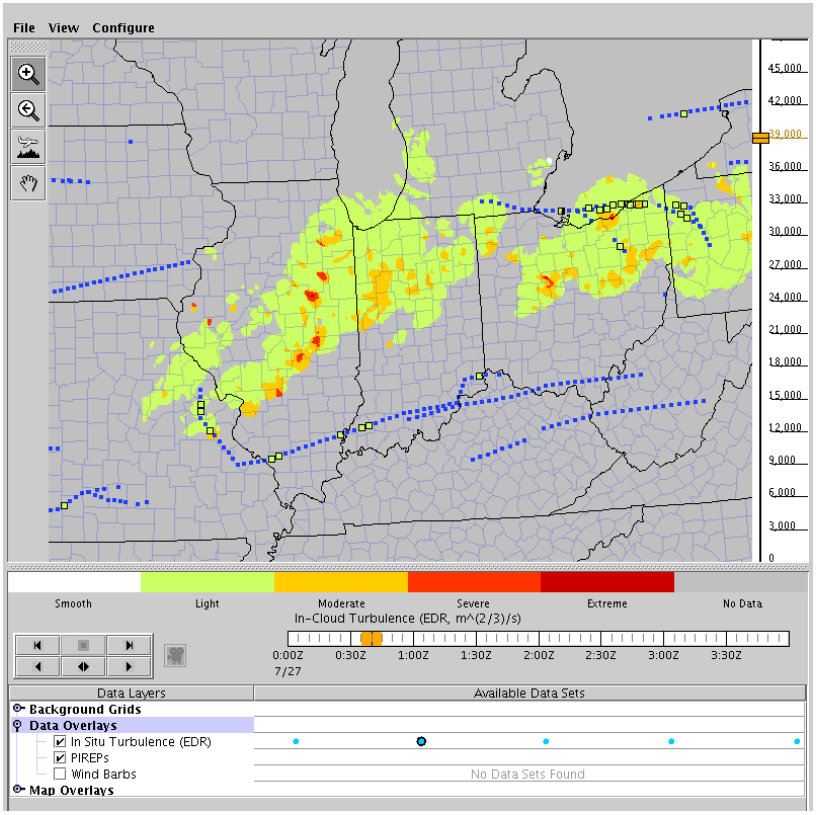

Figure 8: Interactive Java display for disseminating the NTDA operational demonstration data, shown for 0:40 UTC on 27 July 2005. Overlaid are *in situ* turbulence values reported by United Airlines B-757 aircraft.

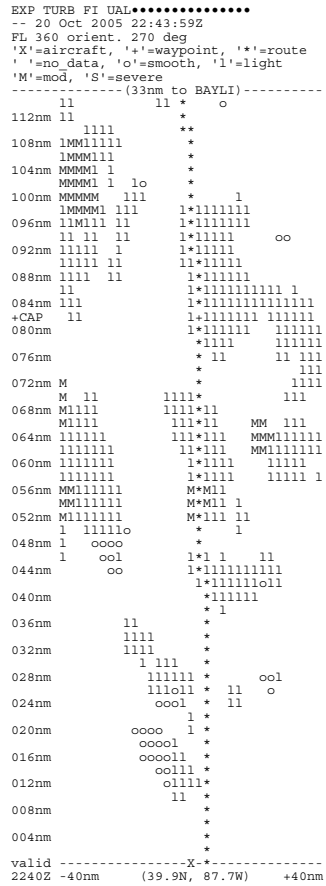

Figure 9: Sample text-based turbulence map generated for a flight from Washington Dulles to San Diego on 20 October 2005. The initial aircraft location is indicated by the X near the bottom, asterisks denote the filed route, and waypoints are indicated by a "+" along the route and labeled in the left margin, which also shows distance in nm along the expected path. Turbulence intensities are denoted by "o" (smooth), "l" (light), "M" (moderate) and "S" (severe).

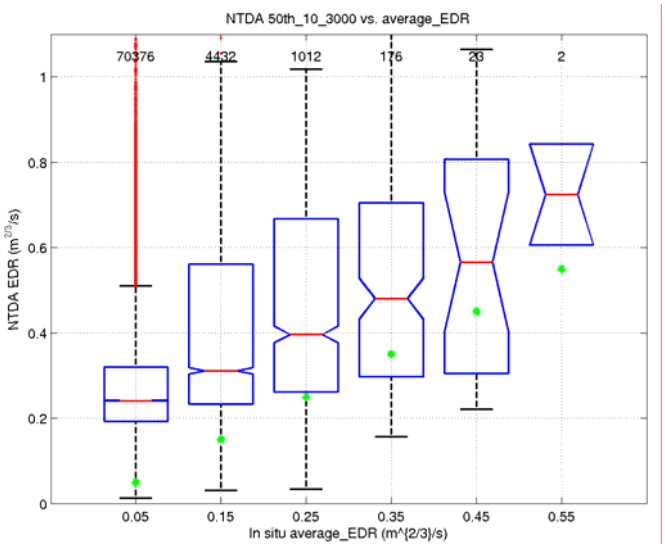

Figure 10: Box plots indicating the distribution of NTDA EDR 3-D mosaic values (the median over the comparison volume described in the text) for different values of *in situ* "average" EDR measurements, shown along the *x*-axis. The horizontal red line in the middle of each "box" indicates the median value, while the upper and lower limits of the box represent the 25th and 75th percentiles, the "whiskers" on either end show the data range, and red dots indicate outliers. Notches in the boxes depict the uncertainty in the median value. The number of data points used in creating each box plot are shown above the box.

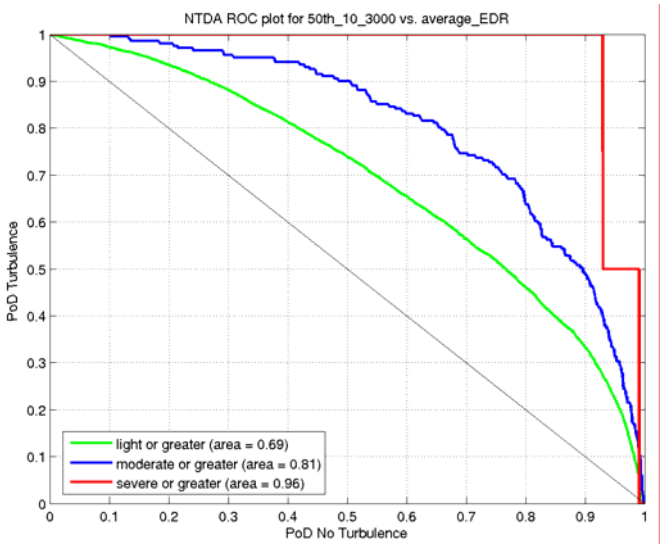

Figure 11: Receiver Operating Characteristic (ROC) curves for light or greater (*in situ* EDR > 0.10 $m^{2/3}$ s^{-1}, green), moderate or greater (*in situ* EDR > 0.30 $m^{2/3}$ s^{-1}, blue), and severe (*in situ* EDR > 0.50 $m^{2/3}$ s^{-1}, red) turbulence. These plots show the tradeoff between the probability of detecting turbulence (*y*-axis) and the probability of detecting no turbulence (*x*-axis) as the NTDA EDR threshold is varied.

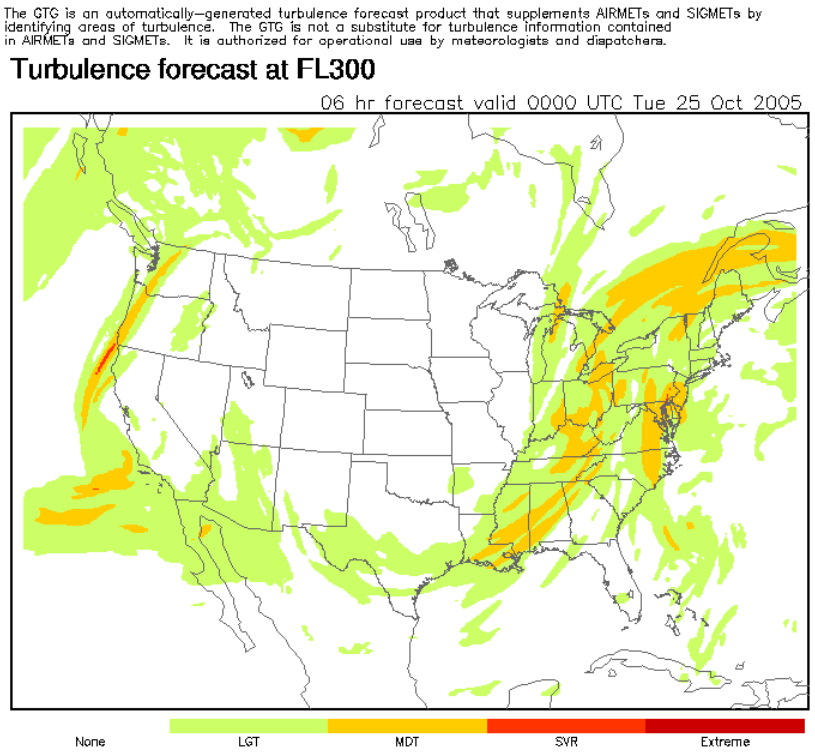

Figure 12. Sample of GTG1 6 hour forecast of CAT potential for 0 UTC 25 Oct 2005 at FL300 as provided on the operational ADDS website (http://adds.aviationweather.gov/turbulence). Color table for contours is provided at the bottom of the image. For this particular situation no turbulence is predicted over most of the western and midwestern U. S., with some light to moderate turbulence regions expected on both the east and west coasts, and possibly a small region of moderate to severe turbulence off the northern California coast.

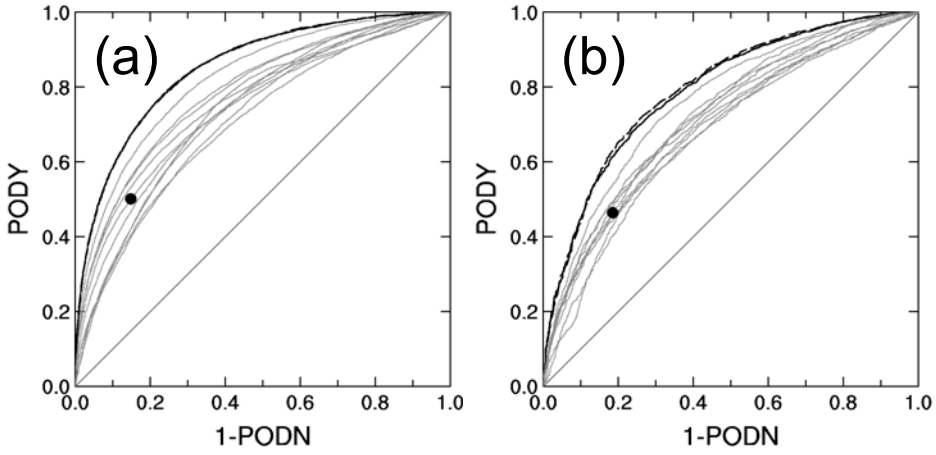

Figure13. Individual diagnostics and the GTG2 PODY-PODN performance statistics (individual diagnostics in thin grey, GTG combination in heavy, black solid and GTG combination using climatological weights in heavy black dashed) derived from one year (2003) of (a) upper-level (FL200-FL460) (b) mid-level (FL100-FL200) 6-hour forecasts (valid 00 UTC). For comparison, also shown is the no skill line as the diagonal, and the 2003 average AIRMET performance (with amendments) at upper levels centered on 00 UTC.

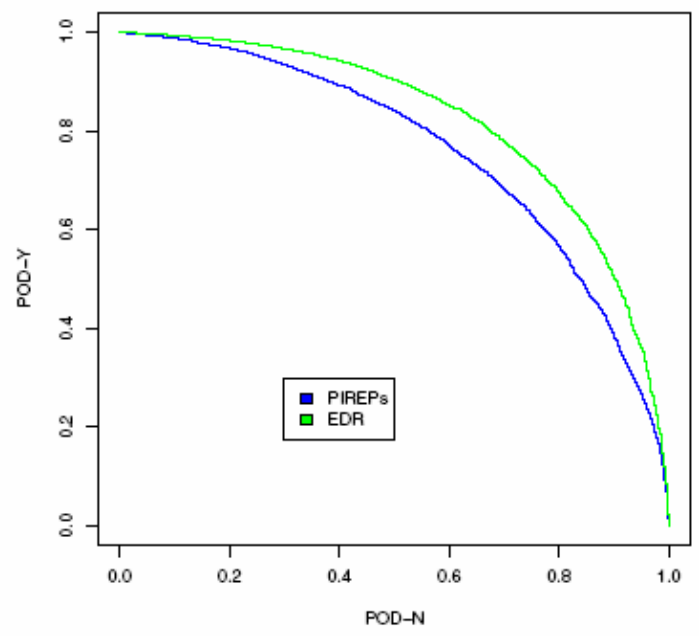

Figure 14. Comparison of GTG2 PODY-PODN performance statistics using only PIREPs (blue) and only *in situ* data (grren) in the GTG2 combination and for verification.

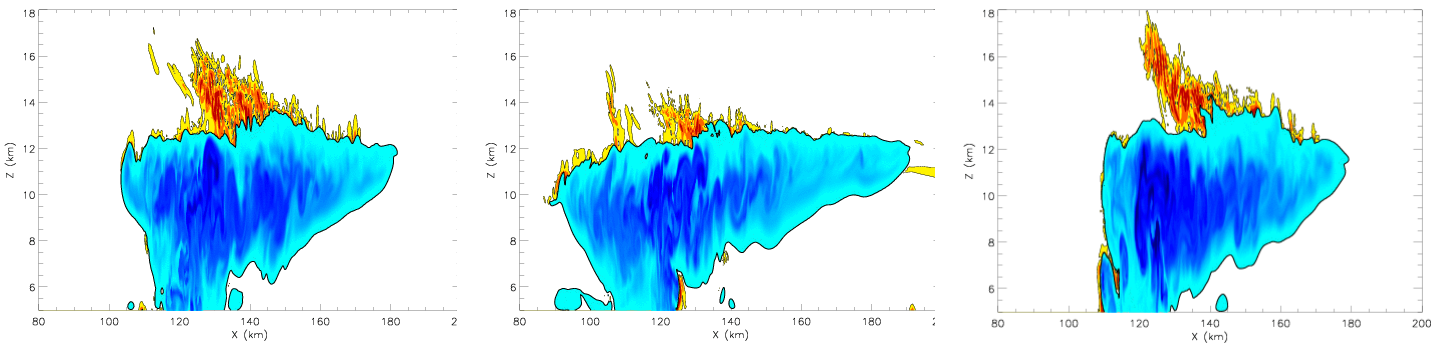

Figure 15. High resolution cloud simulations and CIT above cloud top for three different atmospheric environments. Blue shading denotes cloud concentrations. Yellow, orange, and red shading denotes regions with out-of-cloud total turbulent kinetic energy (TKE) greater then 0.1, 0.5, and 2.0 m^2/s^2, respectively. Left panel: Baseline case using the observed Dickinson, ND encounter environment. Middle panel: Dickinson sounding modified to increase the vertical wind shear near the cloud top. Right panel: Dickinson sounding modified to reduce the static stability at cloud top.

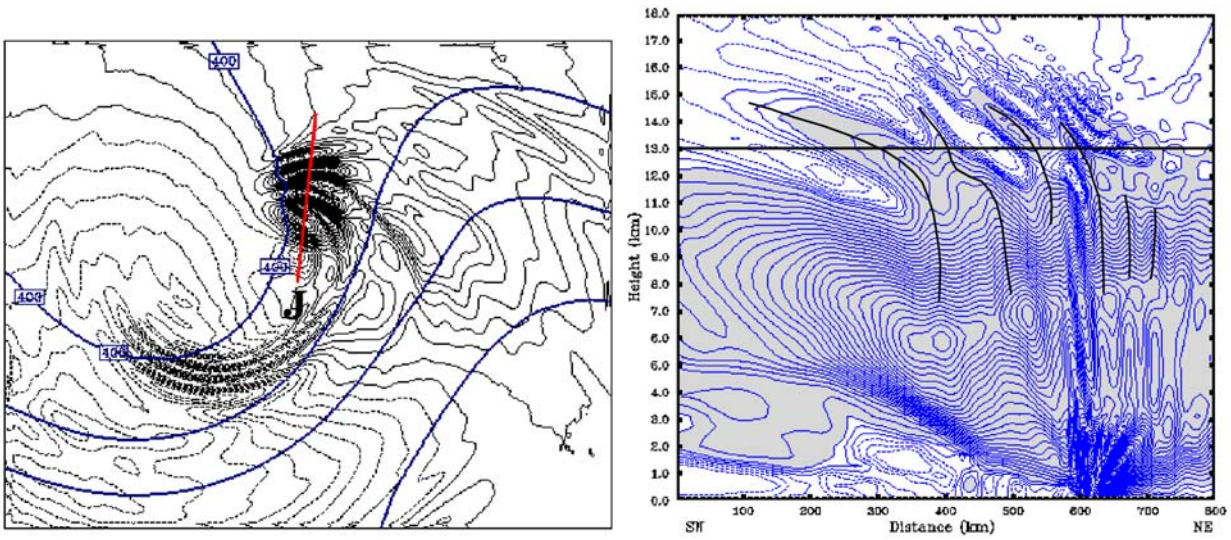

Figure 16. Modeled gravity waves from idealized 10-km grid resolution model: a) vertical velocity (thin-black contours) and potential temperature (thick-blue curves) at 13-km altitude at forecast time 112h, and b) vertical cross-section of vertical velocity (thin-blue curves) and gravity wave fronts (black curves). The red lines in a) and b) indicate the paths of the vertical cross-section.